Electronic Supplementary Information

Constructing Energetic Coordination Polymers through Mixed-Ligand Strategy: Way to Achieve Reduced Sensitivity with Significant Energetic Performance

Priyanka Singla,[a,b] Pramod Kumar Soni,[b] Arjun Singh[*b] and Subash Chandra Sahoo[*a]

[1]Department of Chemistry, Panjab University, Chandigarh 160014, India. *Email: subash.chem@gmail.com
[2]Terminal Ballistics Research Laboratory, DRDO, Chandigarh 160030, India. *Email: arjun.sngh@yahoo.com

Table of contents **Page No.**

Instrumental Details for Characterization

The Powder X-ray diffractometer (PXRD) patterns of the metal CPs were recorded through a X'PERT PRO X-ray diffractometer (PANalytical, Netherlands) employing Cu (wavelength = 1.54184 Å) as anode material and Kα (0.1 nm) (CuKα radiation source) and generator setting at 40 kV and 50 mA. The XRD scanning range of 2 theta (2θ) was adjusted within 10 - 50 degree. FT-IR spectra were recorded in the spectral region of 4000-500 cm^{-1} using a Fourier transform infrared spectroscopy as supplied by Nicolet Avatar 360 using KBr pellets. The samples were grounded with dried KBr powder before pressed into KBr pellets using a hydraulic press. Friction Sensitivity and Impact Sensitivity were tested by Bruceton staircase up down method using BAM Friction Apparatus FSKM-10 and OZM Research BAM Fall Hammer BFH-12 respectively. For friction sensitivity testing, 30-33 mg sample was evenly spread on the porcelain plate, and the frictional force was produced by dragging standard BAM weights across the sample. For impact sensitivity test, the sample was pressed between two steel caps while a standard weight was dropped from various heights. Impact sensitivity was expressed in terms of height from which standard weight dropped on a sample with 50% probability of explosion. Thermal study was carried out through TGA and DSC (Mettler Toledo International Inc., GmbH, Switzerland, model TGA/DSC 1). For thermal stability, the samples were ramped to 25-600 °C at heating rate of 10 °C min^{-1} under flow rate of nitrogen gas 40 mL min^{-1}. For each measurement, 4-6 mg of the sample was taken in an alumina crucible. For kinetic analysis, the samples were subjected to the thermal decomposition at three heating rates; 10, 20 and 30 °C min^{-1} under nitrogen atmosphere. The thermal characteristic data was interpreted by using STARe Software version 11.00 system. The combustion energy at constant volume was determined by using Parr 6200 oxygen bomb calorimeter. A pellet for mixture of CPs and benzoic acid in 1:3 ratio was pressed by hydraulic press. The oxygen bomb calorimeter was calibrated by using pellet of 1 gram of certified benzoic acid. (Standard reference material, 39i, NIST). UV-Vis spectra were recorded on JASCo V-530 UV-Vis spectrophotometer within the range of 200-900 nm using water as reference solvent with scan rate of 400 nm s^{-1}. SEM images were collected on Calro Zeiss (SEM Evo 5 Model). ^{1}H and ^{13}C NMR spectra was recorded on Bruker 500 MHz advance – II spectrometer in DMSO solvent using TMS as internal reference. CHN elemental analysis was carried out on Thermo Sceintific Flash 2000 organic elemental analyser.

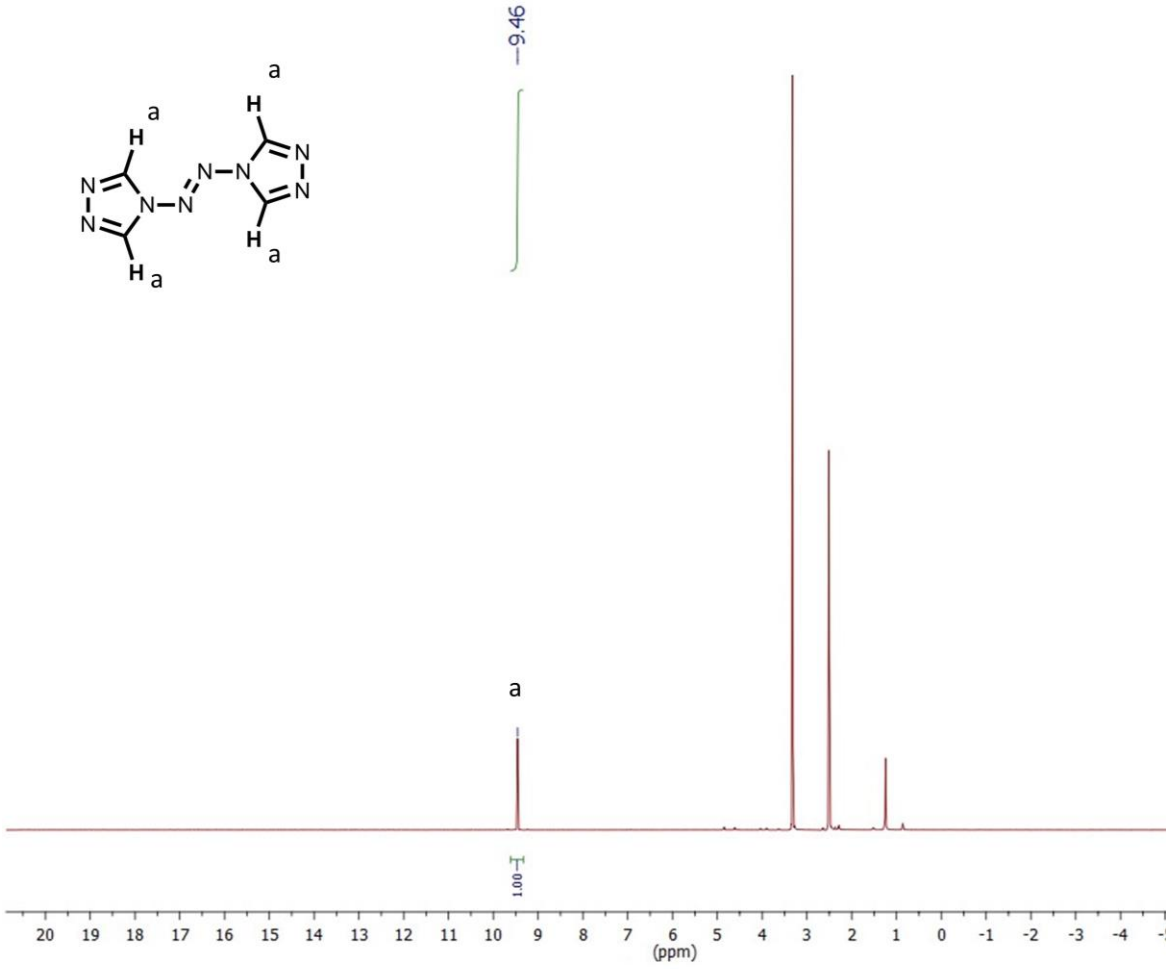

Fig. S1 ^{1}H NMR of ligand atrz in DMSO-d_6 solvent.

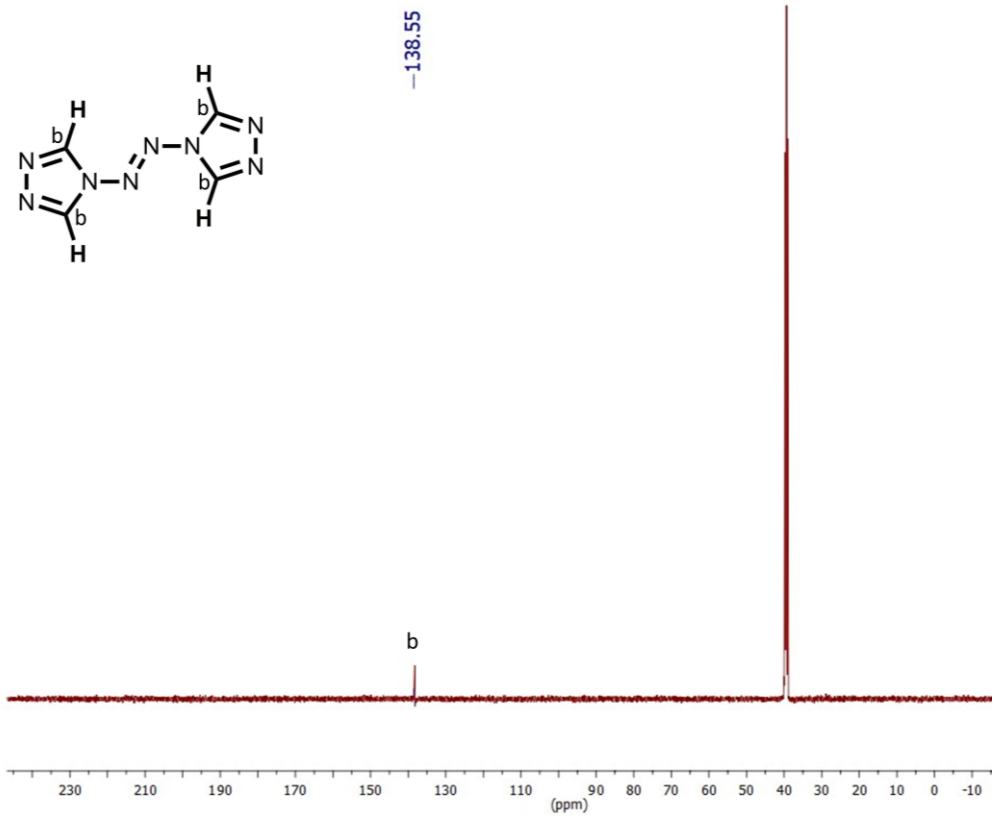

Fig. S2 ^{13}C MNR of ligand atrz in DMSO-d_6 solvent.

Table S1 Crystal data and structural refinement of **1** and **2**.

Crystal parameter	**1**	**2**
CCDC No	2266710	2266709
Empirical Formula	$C_9H_7N_6O_7Zn_{0.5}$	$C_9H_7N_6O_7Cd_{0.5}$
Formula Weight	343.89	367.41
T (K)	293(2)	293(2)
Wavelength (Å)	Mo Kα (λ = 0.71073)	Mo Kα (λ = 0.71073)
Crystal system	Monoclinic	Monoclinic
Space group	$P2_1/n$	$P2_1/n$
a, (Å)	10.59	10.78
b, (Å)	5.32	5.43
c, (Å)	22.33	22.49
V, (Å^3)	1259.22	1318.97
z/p	4/1.814	4/1.850
μ (mm^{-1})	1.075	0.923
Collected reflections	16449	12582
Independent reflections	2748	2771
F(000)	696.0	732
GOF	1.054	0.901
final *R* indices [$I > 2\sigma(I)$]	R_1 = 0.0342, wR_2 = 0.0902	R_1 = 0.0351, wR_2 = 0.0767
R indices (all data)	R_1 = 0.0419, wR_2 = 0.0940	R_1 = 0.0476, wR_2 = 0.0868

Table S2 Selected bond lengths (Å) and bond angles (°) of **1** and **2**.

Selected bond lengths (Å) in **1** and **2**			
Bond Lengths	**(Å)**	**Bond Lengths**	**(Å)**
Zn1O1	2.1533	Cd1O1	2.317
Zn1O11	2.1533	Cd1O11	2.317
Zn1O71	2.1141	Cd1O71	2.313
Zn1O7	2.1141	Cd1O7	2.313
Zn1N3	2.1359	Cd1N3	2.292
Zn1N31	2.1359	Cd1N31	2.292
Selected bond angles (°) in **1** and **2**			
Bond Angles	**(°)**	**Bond Angles**	**(°)**
O1[1]Zn1O1	180.0	O1[1]Cd1O1	180.0
O7Zn1O1	91.32 (6)	O7Cd1O1	90.70 (8)
O7[1]Zn1O1	88.67 (6)	O7[1]Cd1O1	89.30 (8)
O7[1]Zn1O1[1]	91.33 (6)	O7[1]Cd1O1[1]	90.70 (8)
O7Zn1O1[1]	88.68 (6)	O7Cd1O1[1]	89.30 (8)
O7[1]Zn1O7	180.0	O7[1]Cd1O7	180.0
O7[1]Zn1N3[1]	89.85 (7)	O7[1]Cd1N3[1]	89.25 (9)
O7[1]Zn1N3	90.14 (7)	O7[1]Cd1N3	90.75 (9)
O7Zn1N3	89.86 (7)	O7Cd1N3	89.25 (9)
O7Zn1N3[1]	90.15 (7)	O7Cd1N3[1]	90.75 (9)
N3Zn1O1	92.45 (6)	N3Cd1O1	94.25 (9)
N3[1]Zn1O1[1]	92.45 (6)	N3[1]Cd1O1[1]	94.25 (9)
N3ZnO1[1]	87.55 (6)	N3Cd1O1[1]	85.75 (9)
N3[1]Zn1O1	87.55 (6)	N3[1]Cd1O1	85.75 (9)
N3Zn1N3[1]	180.0	N3Cd1N3[1]	180.0

[1]1-X,1-Y,1-Z

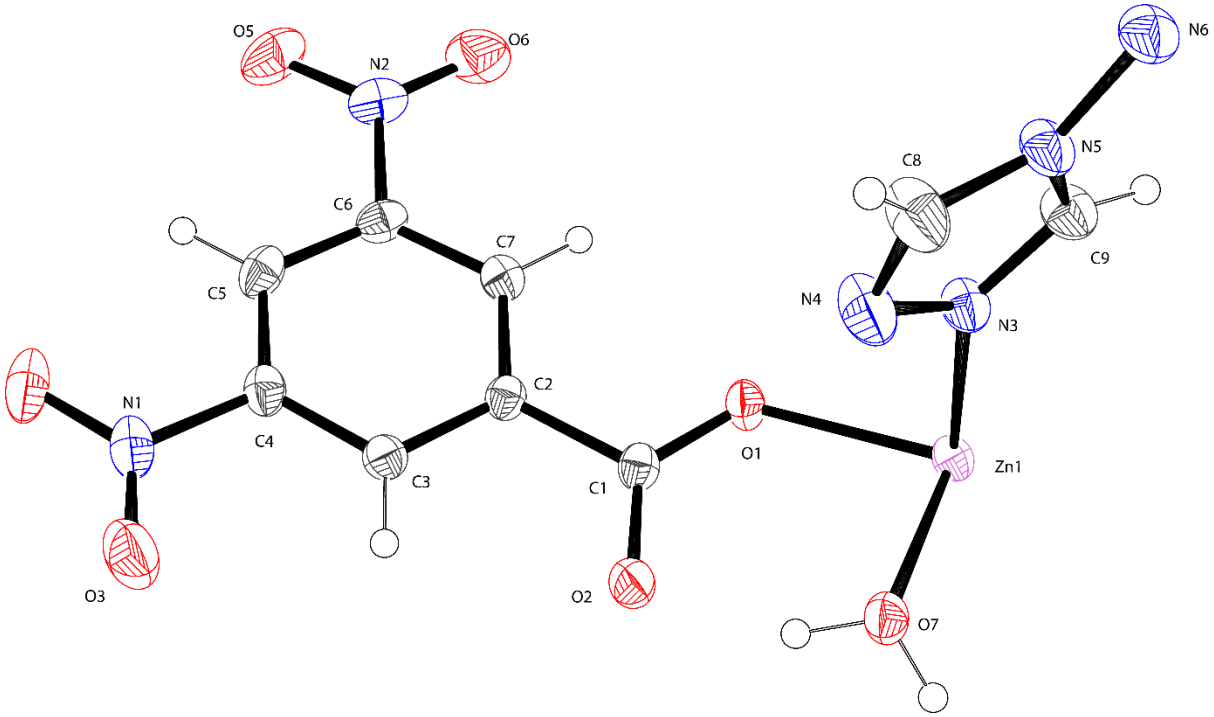

Fig. S3 ORTEP diagram of asymmetric unit of **1** with 40% ellipsoid probability.

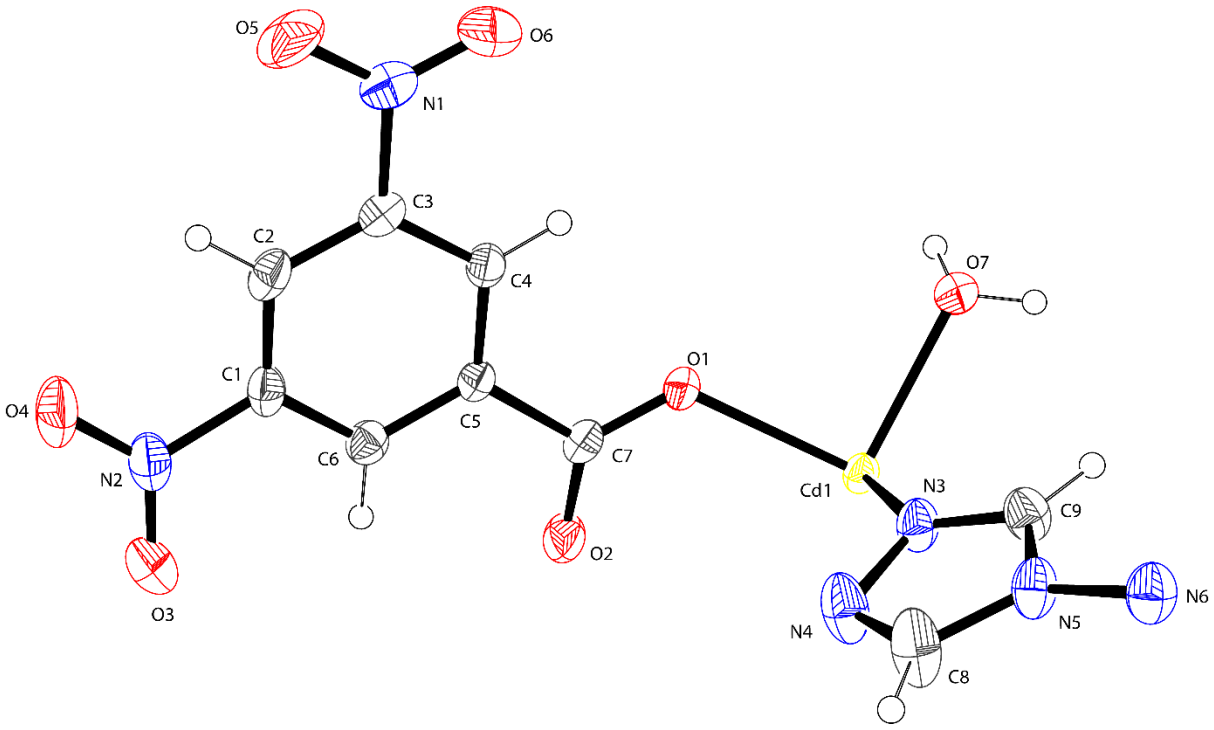

Fig. S4 ORTEP diagram of asymmetric unit of **2** with 40% ellipsoid probability.

Table S3 Hydrogen bond lengths (Å) and angles (°) in **1** and **2**.

CPs	D-H···A	d(D-H)	d(H···A)	d(D···A)	∠DHA
1	O7-H7B···O2	0.867	1.829	2.614	149.56
	O7-H7B···O1	0.867	3.049	2.917	90.41
2	O7-H7B···O2	0.884	1.894	2.673	145.80
	O7-H7A···O1	0.884	2.060	2.849	148.23

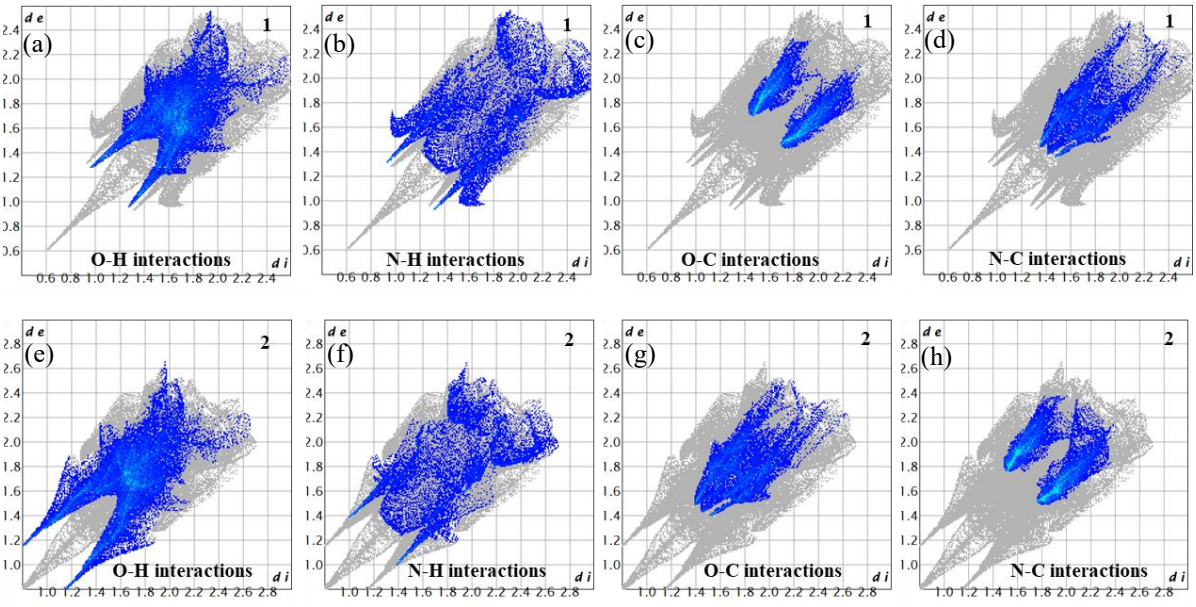

Fig. S5 2D Fingerplot for individual interactions (a-d) in **1** and (e-f) in **2**.

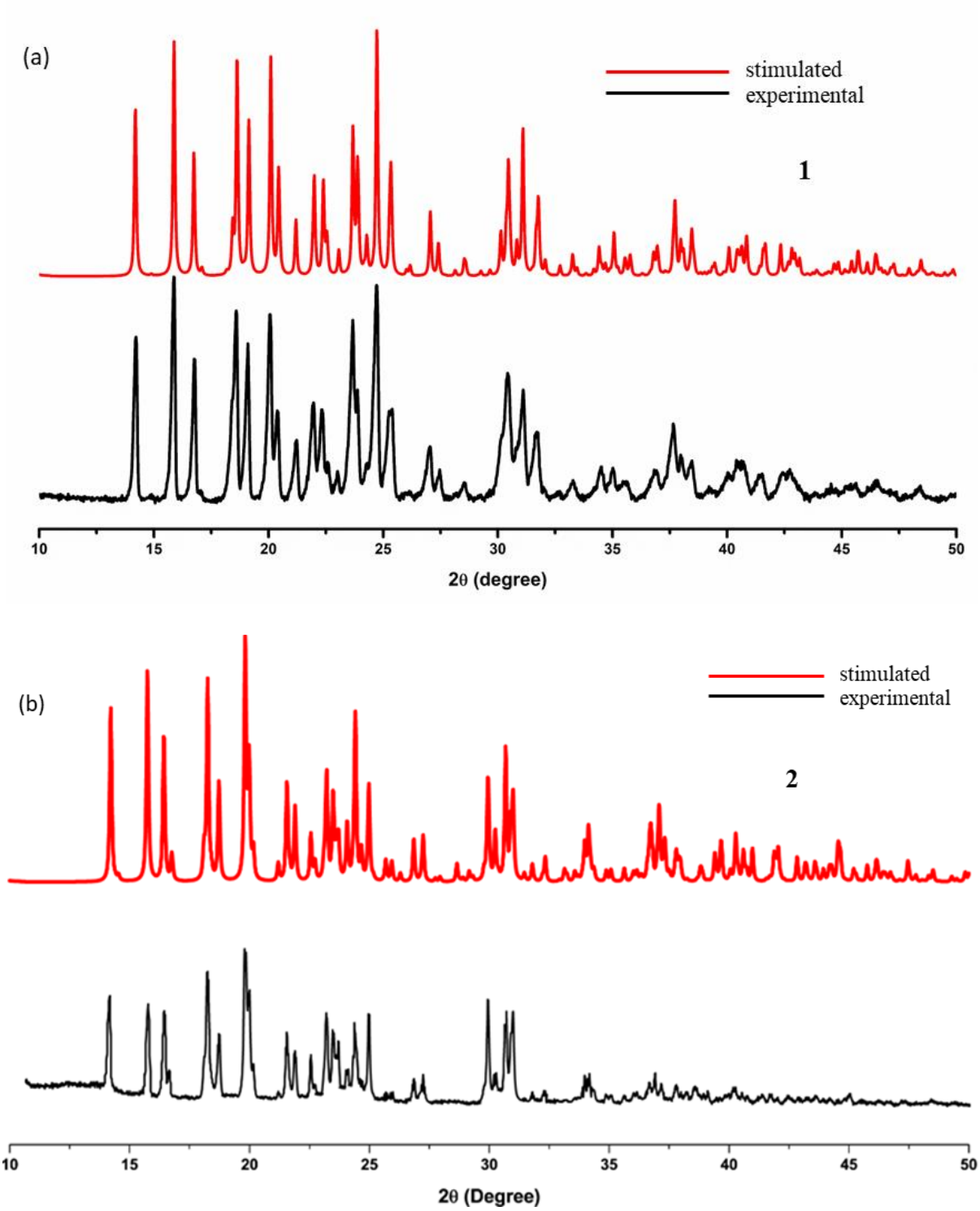

Fig. S6 PXRD patterns of (a) **1** and (b) **2**.

FT-IR study

The FT-IR spectrum of atrz, **1** and **2** is represented in figure S7. In CP **1,** the weak peaks at 3136 and 3053 cm^{-1} correspond to -OH group of water molecules while strong peak at 1605 cm^{-1} attributes to the presence of -C=O group. The presence of NO_2 is indicated by the strong peaks at 1532 and 1504 cm^{-1}. The peak at 1485 cm^{-1} is due to C=N stretching vibrations. The strong peak at 1384 cm^{-1} represents -CH bending vibrations while peaks at 1304 and 1183 cm^{-1} represent bending vibrations of -OH group in **1**. The strong peak at 1033 cm^{-1} is appeared due to the stretching vibrations of -C-O functional group in **1**. The peak at 867 cm^{-1} corresponds to C=C bending vibrations while peak at 711 cm^{-1} confirms the presence of bending vibrations of -CH functional group present in **1**.

The peaks at 3107 and 3083 cm^{-1} confirms the presence of -OH group present in **2** whereas the characteristic peaks at 1698 and 1628 cm^{-1} represent stretching vibrations of -C=O group as shown in FT-IR spectrum of **2** in figure S7. The strong peaks at 1535 and 1497 cm^{-1} indicate -NO_2 stretching vibrations which peak at 1474 cm^{-1} is appeared due to the stretching vibrations of -C=N functional group. The strong peaks at 1343 and 1287 cm^{-1} correspond to the -OH bending vibrations. The presence of -C-O functional group is confirmed by characteristic peak at 1033 cm^{-1}. The peak at 923 cm^{-1} is appeared due to C=C bending vibrations while peak at 720 cm^{-1} represents bending vibrations of -CH functional group.

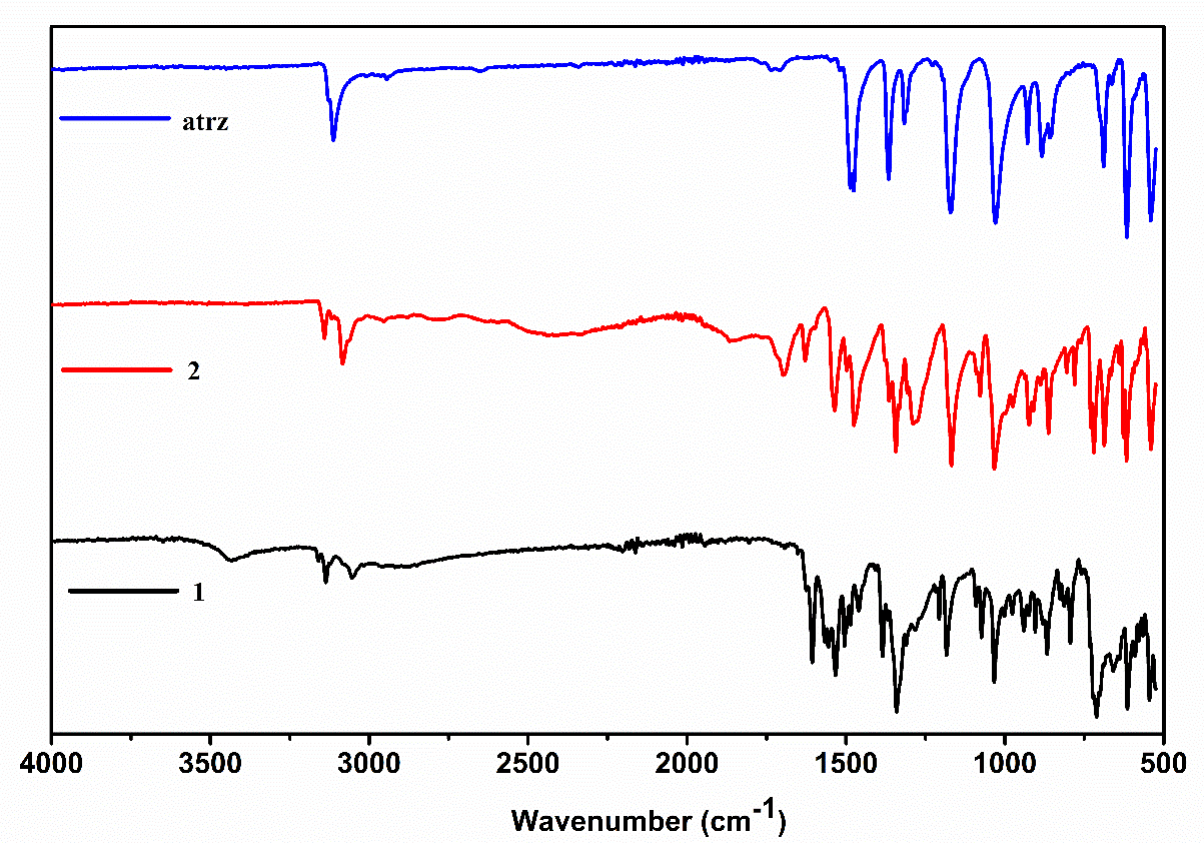

Fig. S7 FT-IR spectrum of atrz, **1** and **2**.

UV Study

The UV-Visible spectra of both ligands (HDNBA and atrz), **1** and **2** were recorded in water solvent shown in figure S8. Due to $\pi \rightarrow \pi^*$ transitions, the atrz exhibits sharp peak λmax at 248 nm while the HDNBA exhibits sharp peak λmax at 264 nm. CP **1** shows two distinct peaks at 205 and 248 nm due to $\pi \rightarrow \pi^*$ transitions of atrz and HDNBA ligands respectively. While CP **2** shows two sharp peaks at 205 and 251 nm which are also due to $\pi \rightarrow \pi^*$ transitions of atrz and HDNBA ligands respectively. Both CP **1** and **2** do not show d-d transition peak as Zn and Cd ions are in +2 oxidation state *i.e.* d^{10} configuration.

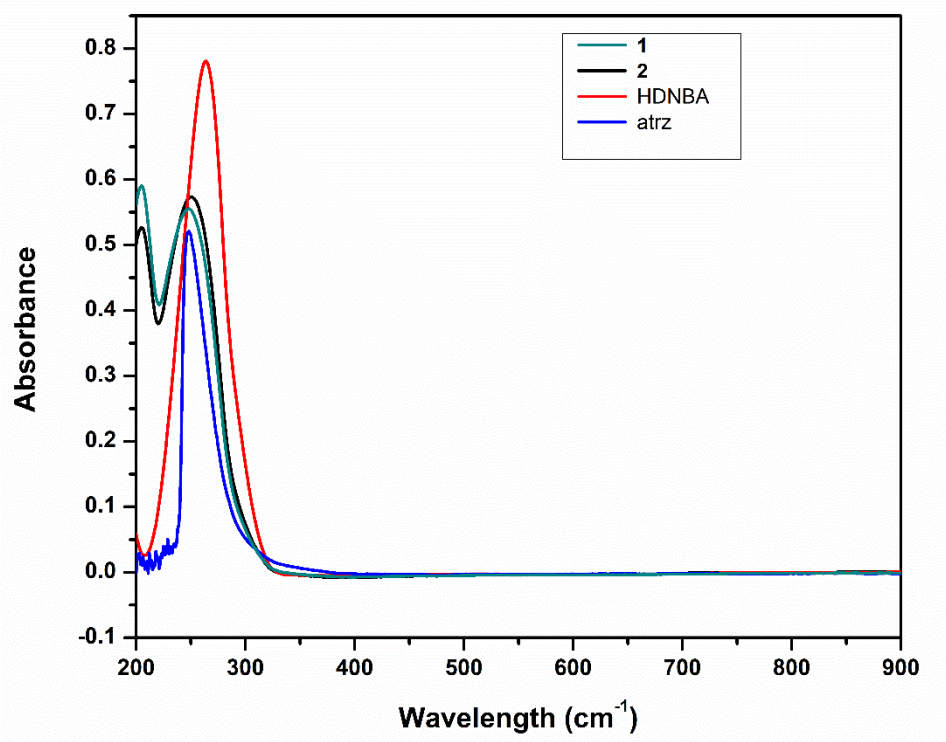

Fig. S8 UV spectrum of atrz, HDNBA, **1** and **2**.

Table S4 Thermal characteristic data of **1** and **2** obtained from DSC method.

CPs	Thermal decomposition temperature (℃)			Enthalpy J/g
	T_{onset}	T_{endset}	T_p	
1st Step				
1	129.9	146.2	137.2	-154.8
2	145.3	160.7	153.3	-141.7
2nd Step				
1	261.7	275.7	268.6	445.3
2	262.6	278.5	269.4	452.5
3rd step				
1	387.6	440.1	424.6	636.3
2	357.1	386.7	365.2	801.9

Table S5 Energetic parameters of **1** and **2**.

	$\Delta_c U^{\theta}_m$ kJ mol^{-1}	$\Delta_c H^{\theta}_m$ kJ mol^{-1}	$\Delta_f H^{\theta}_m$ kJ mol^{-1}	N mol g^{-1}	M g mol^{-1}	Q kcal g^{-1}	ϕ	P g cm^{-3}	D km s^{-1}	P GPa
1	-8562.33	-8540.02	-894.43	0.0233	26.625	0.810	3.428	1.814	6.28	17.57
2	-11000.58	-10978.27	1635.93	0.0218	26.625	1.551	4.438	1.850	7.24	23.67

Table S6 Activation energy data for **1** and **2**.

S. No.	1		2	
	Conversion (%)	Activation Energy (kJ mol^{-1})	Conversion (%)	Activation Energy (kJ mol^{-1})
2	0.1	103.2	0.1	159.1
3	0.2	129.0	0.2	178.2
4	0.3	146.7	0.3	187.5
5	0.4	156.9	0.4	188.1
6	0.5	161.2	0.5	183.2
7	0.6	161.4	0.6	177.3
8	0.7	157.2	0.7	164.7
9	0.8	147.4	0.8	148.0
10	0.9	131.0	0.9	126.2
Mean		143.8		168.0